Size-Dependent Mutual Charge Transfer between B- and P-Codoped Si Quantum Dots and Monolayer MoS2

Wang, Yinggang
Sugimoto, Hiroshi
Fujii, Minoru

(Citation)
Journal of Physical Chemistry C,126(38):16401-16408

(Issue Date)
2022-09-29

(Resource Type)
journal article

(Version)
Accepted Manuscript

Size-dependent Mutual Charge Transfer between B and P codoped Si Quantum Dots and Monolayer MoS_2

Yinggang Wang, Hiroshi Sugimoto and Minoru Fujii**

Department of Electrical and Electronic Engineering, Graduate school of Engineering, Kobe University, Rokkodai, Nada, Kobe 657-8501, Japan

ABSTRACT

Heterostructures built from two-dimensional (2D) transition metal dichalcogenide (TMD) monolayers and quantum dots (0D) offer a large variety of systems for probing the fundamental physics and for the device applications. In this work, 2D/0D heterostructures comprised of monolayer MoS_2 (1L-MoS_2) and Si quantum dots (QDs) are produced and the mutual charge transfer is studied. It is shown that the charge transfer property depends strongly on the size of Si QDs. Decoration of a 1L-MoS_2 flake with Si QDs 3.5 nm in diameter results in the quenching of the PL, while the decoration with Si QDs 9.0 nm in diameter enhances it. The results indicate that the direction of the charge transfer is different depending on the Si QD diameter. Contributions of

the A excitons, B excitons, biexcitons and trions to total PL spectra are analyzed in a wide excitation power range and the mechanism of the charge transfer is discussed.

INTRODUCTION

Two-dimensional transition metal dichalcogenides (TMDs) are an emerging class of materials with properties that make them highly attractive for fundamental studies of novel physical phenomena and for applications ranging from nanoelectronics and nanophotonics to sensing and actuation at the nanoscale. Reducing the thickness of TMDs to a monolayer turns the indirect bandgap semiconductor into a direct bandgap one with the enlarged bandgap due to the quantum confinement effect.[1-4] This makes a monolayer MoS_2 (1L-MoS_2) promising for various optoelectronic applications, such as a light-emitting diode, a laser diode, a photodetector and a solar cell.[5-8] One of the characteristic features of 1L-MoS_2 is the large exciton binding energy in the range of hundreds of meV.[9-12] Because of the large exciton binding energy, trions, biexcitons, and even higher-lying exciton-trion complexes can exist even at room temperature,[13-17] and they govern the luminescence spectra under high excitation power.[18,19]

The property of a monolayer TMD can be strongly modified by the formation of a two dimensional / zero dimensional (2D/0D) heterostructure with semiconductor quantum dots (QDs), and a variety of heterostructures have been produced to improve the performance of TMD-based optoelectronic devices.[20-23] For example, Wu, et al. realized an ultrasensitive photodetector by integrating $CsPbI_{3-x}Br_x$ perovskite QDs with monolayer MoS_2.[21] Tao, et al. hybridized $CuInSe_2$ QDs with monolayer MoS_2 forming a high-performance broadband photodetector.[22] Similar MoS_2-based 2D/0D heterostructures have been produced for a variety of QDs such as GaAs QDs[24] and Si QDs.[25]

In this paper, we study the charge transfer interaction between 1L-MoS_2 and Si QDs with different sizes by the photoluminescence (PL) spectroscopy under different excitation power. We demonstrate that PL of a 1L-MoS_2 flake is strongly suppressed by the decoration with Si QDs 3.5 nm in average diameter, while that is considerably enhanced when it is decorated with those 9 nm in average diameter. These results indicate that the direction of the charge transfer is different depending on Si QD size. From the excitation power dependence of PL spectra deconvoluted into the A exciton, B exciton, biexciton and trion contributions, we discuss the mechanism of the size dependent charge transfer process.

EXPERIMENTAL SECTION

For the formation of a 1L-MoS_2 and Si QDs heterostructure, we used colloidal solution of B and P codoped Si QDs developed in our group.[26,27] The preparation procedure is as follows.[26,27] First, thick Si-rich borophosphosilicate glass (BPSG) films were deposited onto a stainless-steel plate by simultaneously sputtering Si, SiO_2, B_2O_3, and phosphosilicate glass (PSG) (SiO_2 : P_2O_5 =95 : 5 wt%), peeled off from the stainless-steel plate, and annealed in a N_2 gas atmosphere for 30 min to grow B and P co-doped Si QDs in BPSG matrices. The average diameter of Si QDs were controlled by the growth temperature (T_a); T_a= 1100℃, 1200℃, and 1250℃ resulted in the growth of co-doped Si QDs 3.5, 7.0, and 9.0 nm in average diameters, respectively. Si QDs were then extracted from a matrix by hydrofluoric acid (HF) etching and transferred to methanol.

Figure 1a shows a picture of a methanol solution in which Si QDs 7.0 nm in average diameter are dispersed. Since B and P codoped Si QDs are dispersible in polar solvents without agglomeration due to the negative surface potential, the solution is clear and scattering-free.[26,27] Figure 1b shows a transmission electron microscope (TEM) (JEM-2100F, JEOL) image of

codoped Si QDs. For the TEM observation, a diluted methanol solution of Si QDs is dropped on a graphene coated Cu mesh.[30] A film of Si QDs is formed on a graphene sheet. It is important to note that the surface of the Si QDs is not functionalized with organic ligands, and thus efficient charge transfer between QDs is possible. In fact, we have demonstrated that conductive films can be produced simply by drop-coating the methanol solution of co-doped Si QDs on a substrate, and thin film transistors[28] and photoelectrodes[29] are produced by a wet-process.

1L-MoS_2 was prepared by the gold-assisted exfoliation[31] of bulk MoS_2 crystal (HQ-Graphene, Netherlands) and transferred onto a silica substrate 15 mm x 10 mm in size. On the silica substrate, 10μL of methanol solution of Si QDs was dropped and dried in air at room temperature. This results in the formation of 1L-MoS_2 / Si QDs heterostructures on a silica substrate. The concentration of Si QD solution was adjusted so that the amount of Si QDs dropped was enough to cover the whole area of a substrate; the concentrations were 0.09 mg/mL, 0.18 mg/mL, and 0.23 mg/mL for Si QDs 3.5, 7.0, and 9.0 nm in average diameters, respectively. In rough estimation assuming a uniform size and closed-packing of Si QDs, 1L-MoS_2 is covered by an almost monolayer of Si QDs, although the size distribution and the disorder of the alignment affect the coverage slightly.

1L-MoS_2 / Si QDs heterostructures were characterized by PL and Raman scattering spectroscopy. For the PL and Raman scattering measurements, a confocal microscope (50× objective lens, N.A. = 0.8) equipped with a single monochromator and a charge coupled device (Andor SOLIS Newton-CCD) was used. The PL excitation wavelength was 405 nm and the power was changed from 0.01 μW to 5000μW. The excitation wavelength for Raman scattering measurements was 488 nm. All the optical measurements were performed at room temperature.

Figure 1c shows an optical microscope image of a 1L-MoS_2 flake (the region enclosed by a white dashed curve) on which a monolayer of Si QDs is placed. Images of other flakes are shown in the Supporting Information (Figure S1). Figure 1d shows a Raman spectrum of a 1L-MoS_2 flake. Two characteristic Raman peaks assigned to E^1_{2g} and A_{1g} vibrational modes are observed. The separation of the modes is 19.2 cm^{-1}, which corresponds to that of a monolayer 1L-MoS_2. This confirms that 1L-MoS_2 is successfully exfoliated. Figure 1e shows the PL spectrum of an as-prepared 1L-MoS_2 flake, i.e., a 1L-MoS_2 flake without Si QDs on top, excited at 405 nm (2.5 μW). The PL peak is around 1.89eV. This indicates that the PL spectrum is dominated by the A exciton emission.[15,18,32]

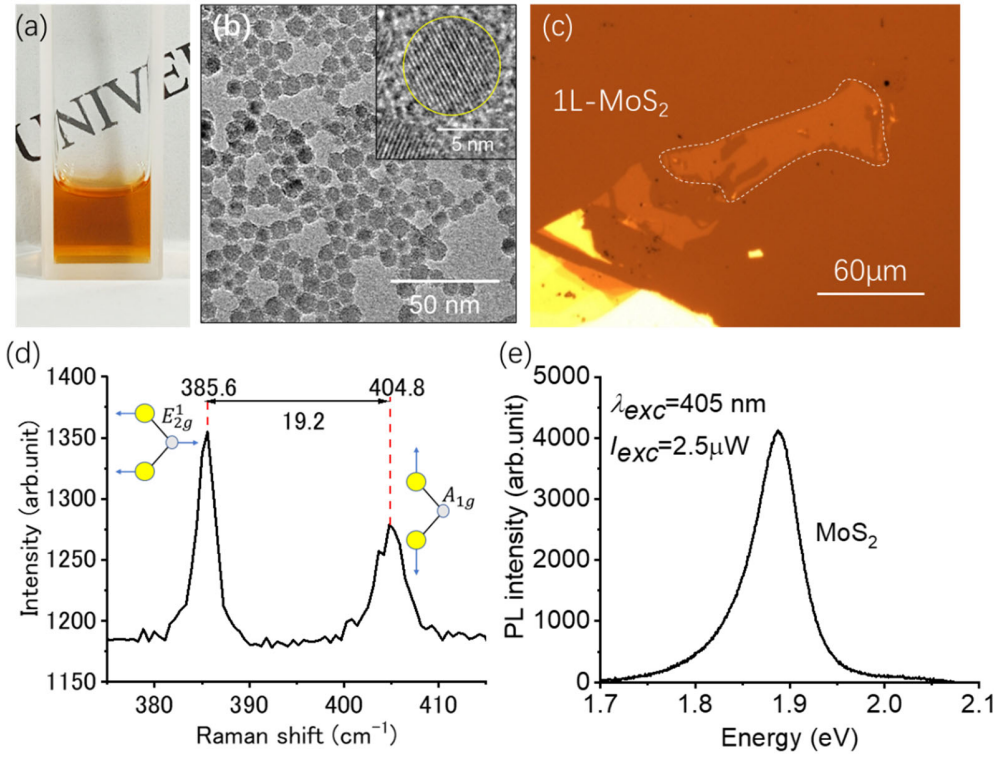

Figure 1. (a) Photograph of methanol solution of B and P codoped Si QDs 7.0 nm in average diameter. (b) TEM image of Si QDs on a graphene support film. (c) Optical microscope image of

a 1L-MoS_2 flake (the region enclosed by a white dashed curve) on which a monolayer of Si QDs is placed. (d) Raman spectrum of a 1L-MoS_2 flake. (e) PL spectrum of 1L-MoS_2 flake before depositing Si QDs on top.

RESULTS AND DISCUSSION

Figure 2 shows PL spectra of a 1L-MoS_2 flake before (black) and after (red) depositing Si QDs. The data obtained for different size Si QDs, i.e., (a) 3.5, (b) 7.0 and (c) 9.0 nm in average diameters, are shown. Ideally, the PL spectra of 1L-MoS_2 flakes on silica before Si QD deposition should be identical for three samples. However, in Figure 2a-c, the intensity and spectral shape are different from a flake to flake. This is due to large variation of defect densities in flakes produced by the gold-assisted exfoliation method. To study the effects of Si QDs without being disturbed by the variation, we first performed all necessary optical measurements for 1L-MoS_2 flakes before Si QD deposition, and then repeated the same measurements for the same flake after depositing a QDs monolayer. Therefore, PL spectra are measured at exactly the same positions before and after Si QD deposition. The excitation wavelength is 405 nm and the excitation power is around 2 μW. Note that PL from Si QDs is much weaker than that of 1L-MoS_2 flakes and is not detectable at the measurement condition. It is also very important to note that, the optical absorbance of a Si QDs monolayer is more than an order of magnitude smaller than that of a 1L-MoS_2 flake at 405 nm (Figure S2 in the Supporting Information) due to the indirect nature of the energy band structure. Therefore, the excitation light is mainly absorbed by 1L-MoS_2, and direct excitation of Si QDs by the excitation light is negligible.

In Figure 2a, simply by depositing Si QDs 3.5 nm in average diameter, the PL is strongly quenched and red-shifts about 16 meV. This suggests that there is efficient charge transfer between

1L-MoS_2 and Si QDs. Similar behavior is observed in Figure 2b for larger Si QDs (D_{ave}=7.0 nm), although the quenching is less serious. On the other hand, in Figure 2c (D_{ave}=9.0 nm), the intensity increases by Si QD deposition and the peak blue-shifts. Therefore, different size Si QDs affect the PL property of 1L-MoS_2 differently.

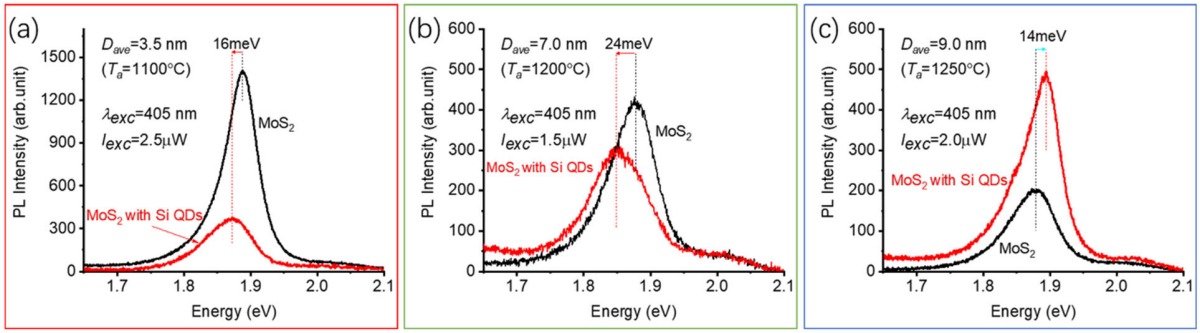

Figure 2. PL spectra of 1L-MoS_2 flakes without (black) and with (red) Si QDs excited at low excitation power (<2.5 μW). The peak energies are marked with dash lines. (a) D_{ave}=3.5 nm, (b) D_{ave}=7.0 nm, and (c) D_{ave}=9.0 nm. The growth temperatures (T_a) of Si QDs are shown below the size description.

To study the mechanism of the PL modulation by Si QD deposition, we measure the excitation-power dependence of the PL spectra both before and after Si QD deposition (Figure S3 in the Supporting Information). Figure 3a and b shows the PL peak energy and the full width at half maximum (FWHM) before and after depositing Si QDs 3.5 nm in average diameters, respectively, as a function of the excitation power. The excitation wavelength is 405 nm. Similar data for other samples are shown in the Supporting Information (Figure S4). In both cases, i.e., with and without Si QDs, the peak red-shifts and becomes broad with increasing the excitation power. This is due to the emergence of the PL from biexciton besides A and B excitons and trions.[18,33-36] In Figure

3c, the ratio of PL intensity between 1L-MoS_2 flakes with and without Si QDs are plotted as a function of the excitation power. The ratio depends strongly on the diameter of Si QDs at low excitation power. This suggests that the charge transfer process depends on the size of Si QDs. The ratio approaches unity as the excitation-power increases. This indicates that under strong excitation, photoexcited carriers dominate the PL property of 1L-MoS_2 and charge transfer from/to Si QDs plays a minor role.

In Figure 3a and b, we can see plateaus in the peak energy and the FWHM at a relatively high power range (0.2−1mW). Similar plateaus appear at almost the same energies for other samples with different size Si QDs (Figure S4 in the Supporting Information). The existence of the plateaus indicates that one excitonic state dominates the PL spectra in the excitation power range. From the comparison with the literature values of the peak energy[18,33,37] and the FWHM,[18,38] it is most plausible that emission from biexcitons dominates the PL spectra in the plateaus. From the figures, we determine the peak energy of biexcitons (P_X) to 1.835eV. Similarly, from the plateau at the low excitation power range in Figure 3a and b, the peak energy of A excitons (P_A) is determined to 1.890 eV. These energies and the energy difference between A excitons and biexcitons, i.e., the binding energy of biexcitons (E_{Xb}~55meV), agree well with the literature values.[18,33,37,39]

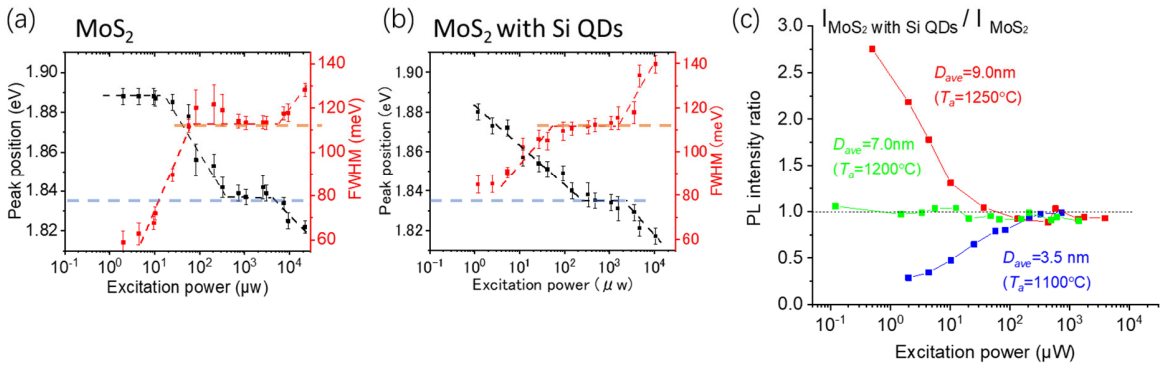

Figure 3. (a, b) Excitation-power dependence of the PL peak energy and the FWHM of a 1L-MoS_2 flake without Si QDs (a) and with Si QDs 3.5nm in average diameter (b). Plateaus in the peak energy and the FWHM are designated by horizontal dashed lines. (c) The ratio of PL intensity between 1L-MoS_2 flakes with and without Si QDs as a function of the excitation power for Si QDs with the average diameters of 3.5 nm (blue), 7.0 nm (green), and 9.0 nm (red). The growth temperatures (T_a) of Si QDs are shown below the size description.

In order to analyze the progression of the PL spectral shape with excitation power, we decompose the spectra into A and B excitons, trions and biexcitons with Lorentzian functions. Figure 4a and b shows the results of deconvolution for a 1L-MoS_2 flake without Si QDs excited at 2.5 and 323 μW, respectively. We fitted the peak with four Lorentzian functions under the assumption that the main peak is composed of A excitons, trions and biexcitons, and the high energy shoulder is composed of B excitons. The peak energies of A excitons and biexcitons are fixed to the above determined values, and those of trions and B excitons and FWHM of all peaks are treated as fitting parameters. By the fittings, the peak energy of trions (P_T) is obtained to ~1.862 eV. This means that the binding energy (E_{Tb}) is ~28meV, which is consistent with the $E_{XXb}/E_{Tb} \approx 2$ relation.[18,39-42] In the Supporting Information (Figure S5), the FWHM of the peaks are shown as a function of excitation power. The FWHM of all the peaks are close to literature values at room temperature.[38,43] Furthermore, the FWHM of the biexciton peak is approximately twice that of the A exciton one, consistent with previous results.[35,38]

In Figure 4c, the result of deconvolution of the PL spectrum of a 1L-MoS_2 flake with Si QDs (D_{ave}=3.5 nm) is shown. The excitation power is the same as that in Figure 4a. The peak energies of A excitons, trions and biexcitons are fixed to the above values and that of the B excitons is

treated as fitting parameters. The peak is very well deconvoluted with the procedure. We can clearly see the decrease of the contribution of A excitons and the increase of that of biexcitons by the Si QD deposition.

Figure 4d shows the integrated intensities (I) of deconvoluted peaks as a function of the excitation power (P) for a 1L-MoS_2 flake without Si QDs. The lines are the results of the fittings by the $I \propto P^{\alpha}$ relation. The value of α obtained by the fittings are shown in the figure. The A exciton emission shows sublinear power dependence (α=0.56) at the low excitation power range and then saturates, while the biexciton PL increases almost linearly (α=1.04). In the Supporting Information (Figure S6), we show the relation between the intensities of biexcitons (I_{Bi}) and A excitons (I_A), and from the $I_{Bi} \propto I_A^n$ relation, n is extracted. The values of n obtained for three different 1L-MoS_2 flakes are in the range of 1.37 to 1.74, in consistent with previously observed values in TMDs (1.2-1.9).[34,42,44,45] The subquadratic relation is usually attributed to the non-equilibrium of biexciton formation and exciton recombination processes.[34,44,45] Figure 4e shows the $I \propto P^{\alpha}$ relation after depositing Si QDs 3.5 nm in average diameter. We can clearly see the decrease of the A exciton emission in the whole excitation power range. Similar data obtained for other samples are shown in the Supporting Information (Figure S7).

By comparing Figure 4d and e, we can clearly see that the intensity of A excitons decreases significantly by Si QD deposition, while those of trions and biexcitons are not strongly affected. Figure 4f-h shows the integrated intensities of A exciton PL with (red curves) and without (black curves) Si QDs 3.5, 7.0 and 9.0 nm in average diameters, respectively. By the deposition of Si QDs 3.5 and 7.0 nm in average diameters, the emission of A excitons is strongly quenched in the whole excitation power range. On the other hand, when Si QDs 9.0 nm in diameter are deposited, the A exciton emission increases at the low excitation power range and decreases at the high

excitation power range. These behaviors of A excitons are similar to that of the total intensity shown in Figure 3. This indicates that the effect of Si QD deposition appears most apparently in the PL intensity of A excitons. In Figure 4f-h, the sudden drop of the A exciton PL intensity is caused by the decrease of the exciton-binding energy due to very high carrier density close to the critical limit for the Mott transition.[46,47]

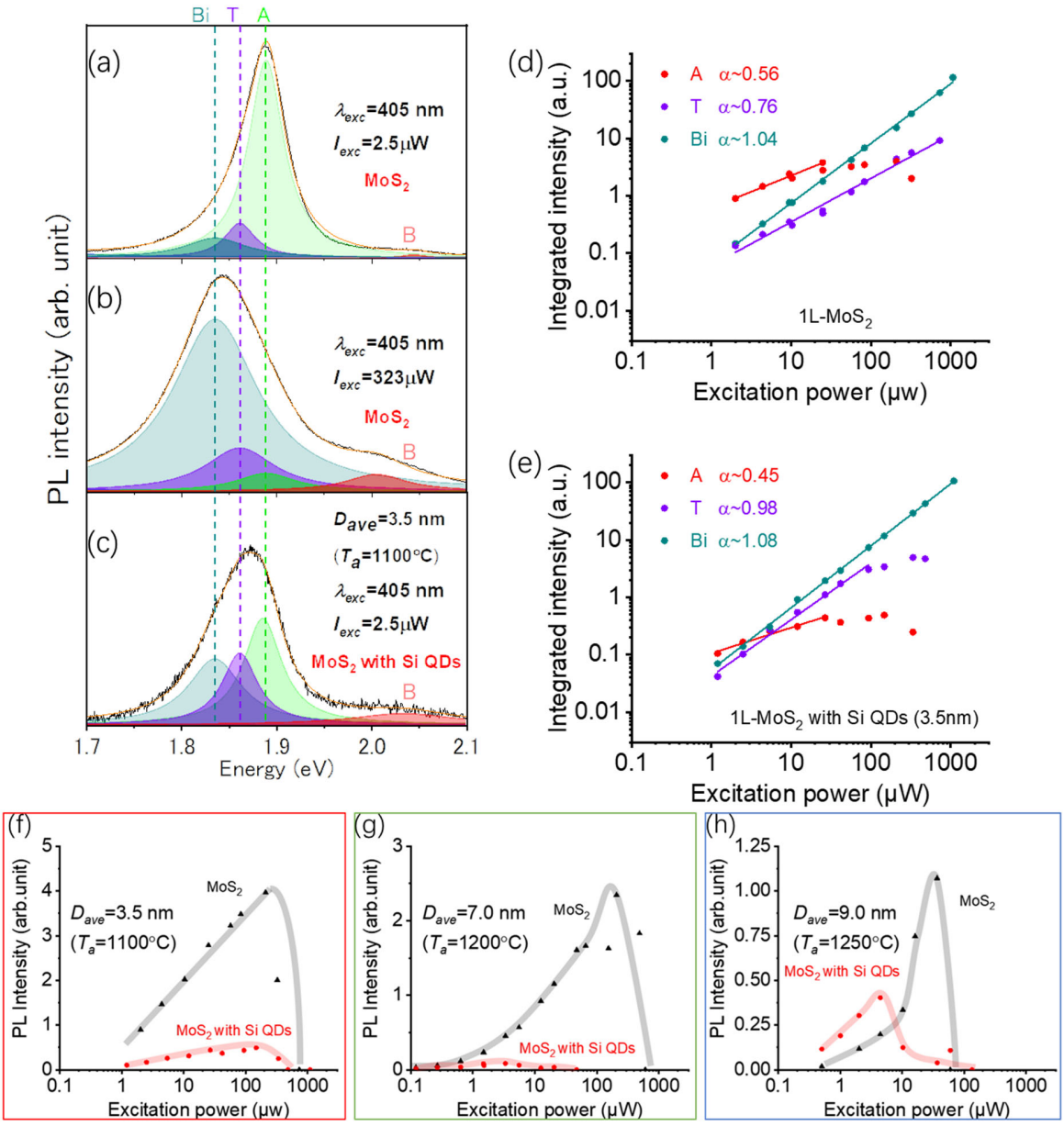

Figure 4. (a, b) PL spectra of a 1L-MoS_2 flake without Si QDs excited 2.5 μW (a) and 323 μW (b). (c) PL spectrum of a 1L-MoS_2 flake with Si QDs 3.5 nm in average diameter on top. In (a-c), the spectra are deconvoluted with Lorentzian functions into contributions of A excitons (A), B excitons (B), trions (T), and biexcitons (Bi). (d, e) Integrated PL intensities of A excitons, trions and biexcitons as a function of excitation power for a 1L-MoS_2 flake without Si QDs (d) and with Si QDs 3.5nm in average diameter (e). The lines are the results of the fittings by the $I \propto P^{\alpha}$ relation. (f-h) Integrated PL intensities of A excitons as a function of excitation power for a 1L-MoS_2 flake without (black triangle) and with (red circle) Si QDs. The average diameter of Si QDs is (f) 3.5 nm, (g) 7.0 nm and (h) 9.0 nm. The curves are guide to the eyes. The growth temperatures (T_a) of Si QDs are shown below the size description.

Based on the experimental results, we now discuss the charge transfer process between 1L-MoS_2 and Si QDs with different diameters at different excitation power regimes. First, we assume that similar to previous works,[22,32,48] 1L-MoS_2 used in this work is n-type. This is consistent with rather strong trion emission without Si QDs at low excitation power. We also assume that excitation light is absorbed mainly by 1L-MoS_2 and photoexcited carriers in Si QDs are negligible. In the case of Si QDs 3.5 nm in diameter, a type II band alignment is expected at a 1L-MoS_2 / Si QD interface as shown in Figure 5a.[48-51] In this band alignment, charge transfer does not occur in dark. Under photoexcitation, excited holes are preferentially transferred to Si QDs, while excited electrons remain in 1L-MoS_2. This charge separation makes 1L-MoS_2 more heavily n-type doped (photo-doping),[32,52,53] which appears as strong quenching of A exciton emission by Si QD deposition. Under strong excitation, the band gap of 1L-MoS_2 is reduced by the band gap renormalization.[32,54]

However, the situation is identical to the case of weak excitation and thus no discontinuity is observed in the excitation power dependence of the A exciton emission (Figure 4f).

In the case of Si QDs 9.0 nm in diameter, the lowest unoccupied molecular orbital (LUMO) level is lower than that of Si QDs 3.5 nm in diameter,[48,49,51,55] and it is expected to be lower than that of 1L-MoS_2. The band alignment is thus considered to be type I as can be seen in Figure 5b.[48-51] In this band alignment, excess electrons in 1L-MoS_2 are readily transferred to Si QDs and the electron density of 1L-MoS_2 decreases.[56,57] As a result, under weak excitation, the A exciton emission is enhanced by depositing Si QDs. Under high power excitation, band gap renormalization mentioned above changes the band alignment to type II, and the situation becomes the same as the case of Si QDs 3.5 nm in diameter. In this situation, n-type photo-doping due to hole transfer from 1L-MoS_2 to Si QDs strongly quenches the A exciton PL. This appears as a cross-over of the A exciton PL intensity between 1L-MoS_2 without and with Si QDs around 10μW in Figure 4h. In the case of Si QDs 7.0 nm in diameter, the band alignment is in between the two extremes, and thus the effect of Si QD deposition is smaller than others as can be seen in Figure 3c.

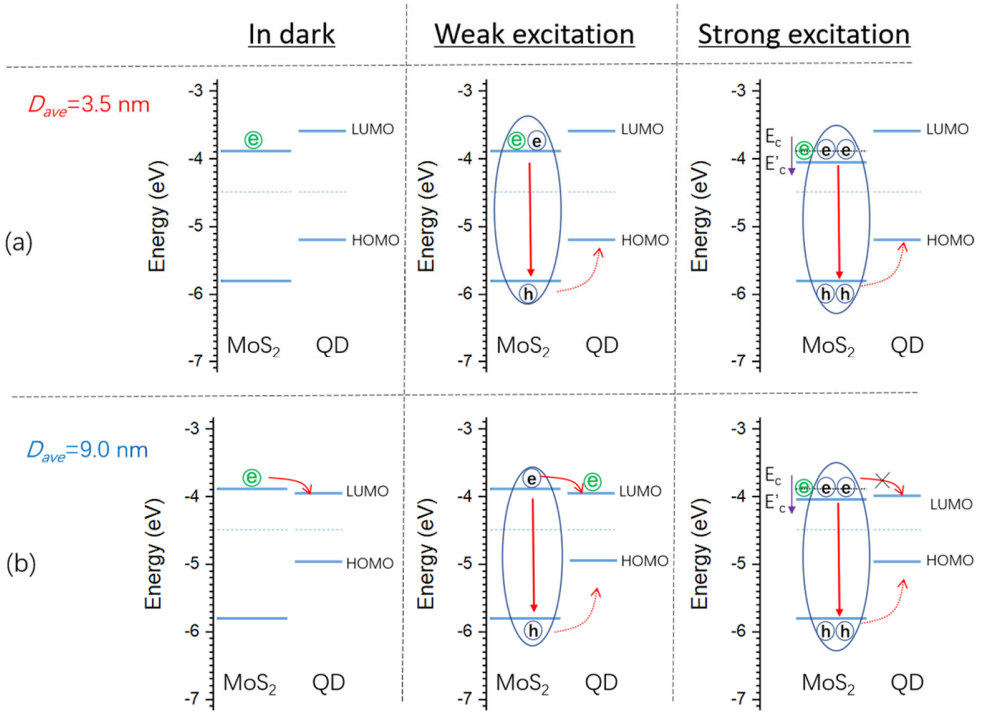

Figure 5. Schematic of band alignment and charge transfer in dark and under low and high power excitation in 1L-MoS_2 / Si QDs heterostructures, (a) 3.5 nm and (b) 9.0 nm in average diameters.

In the above model, we discussed the observed properties based solely on the size of Si QDs. This is a simplified model because strictly speaking, the size of Si QDs affects the crystallinity,[58] dopant concentration, dopant locations,[59] etc., and all of them may affect the energy level structure. However, in B and P codoped Si QDs produced from the same precursor, i.e., the same Si-rich borophosphosilicate glass, the size is considered to be the largest factor to determine the energy level structure.[60] Therefore, we believe that the model shown in Figure 5 explains the essential part of the carrier exchange mechanism.

CONCLUSION

We have studied the charge transfer interaction between 1L-MoS_2 and Si QDs with different sizes. We showed that the PL property of 1L-MoS_2 is strongly modified by placing a monolayer of Si QDs on top and that the effect of Si QDs on the PL property depends strongly on the size. When the diameter is 3.5 nm, the PL is quenched by placing Si QDs, while when the diameter is 9.0 nm, it is enhanced. Deconvolution of the PL spectra into the contributions of A-excitons, trions, biexcitons, and B-excitons revealed that PL from A-excitons is most strongly modified by Si QDs, i.e., the A-exciton PL is quenched by 3.5 nm Si QDs and enhanced by 9.0 nm Si QDs. These effects could be explained from the band alignments. When the diameter of Si QDs is 3.5 nm, the LUMO level is higher in energy than that of 1L-MoS_2 and the band alignment is type II, while when the diameter is 9.0 nm, the relation is vice versa and the band alignment is type I. In the latter case, excess electrons in n-type 1L-MoS_2 are transferred to Si QDs and the density of excess electron decreases. This enhances the A-exciton emission. In the former case, the charge transfer does not occur in dark. Under photoexcitation, excited holes are preferentially transferred to Si QDs, while excited electrons remain in 1L-MoS_2. This charge separation makes 1L-MoS_2 more heavily n-type doping and the A-exciton PL is quenched. The present results indicate that by simply placing Si QDs, carriers in 1L-MoS_2, and thus the optical and electrical properties can be strongly modified. By properly choosing the Si QDs size, the heterostructure can be used for a carrier-separation type device such as solar cells and photodetectors and for a carrier-recombination type device such as LEDs and laser diodes.

ASSOCIATED CONTENT

Supporting Information.

The Supporting Information is available free of charge at https://pus.acs.org/doi/.

Photos of 1L-MoS_2 flakes, absorption spectra of Si QDs monolayers, PL spectra of 1L-MoS_2 without and with Si QDs, excitation-power dependence of the PL peak energy and the FWHM, the FWHMs of A exciton, trion, and biexciton PL peaks for 1L-MoS_2 flakes without and with Si QDs, relation between the PL intensities of biexciton and A exciton, and integrated PL intensities of A excitons, trions and biexcitons as a function of excitation power. (PDF).

AUTHOR INFORMATION

Corresponding Author

*Minoru Fujii − Department of Electrical and Electronic Engineering, Graduate School of Engineering, Kobe University, Kobe 657-8501, Japan; orcid.org/0000-0003-4869-7399;

Email: fujii@eedept.kobe-u.ac.jp

*Hiroshi Sugimoto − Department of Electrical and Electronic Engineering, Graduate School of Engineering, Kobe University, Kobe 657-8501, Japan; orcid.org/0000-0002-1520-0940;

Email: sugimoto@eedept.kobe-u.ac.jp

Author Contributions

The manuscript was written through contributions of all authors. All authors have given approval to the final version of the manuscript.

Acknowledgment

This work was partly supported by JSPS KAKENHI Grant Nos. 18K14092, 18KK0141, and 19K22111.

Notes

The authors declare no competing financial interest.

REFERENCES

1. Wang, Q. H.; Kalantar-Zadeh, K.; Kis, A.; Coleman, J. N.; Strano, M. S. Electronics and Optoelectronics of Two-Dimensional Transition Metal Dichalcogenides. *Nat. Nanotechnol.* **2012,** *7*, 699–712.
2. Zhang, Y.; Chang, T. R.; Zhou, B.; Cui, Y. T.; Yan, H.; Liu, Z.; Schmitt, F.; Lee, J.; Moore, R.; Chen, Y.; et al. Direct Observation of the Transition from Indirect to Direct Bandgap in Atomically Thin Epitaxial $MoSe_2$. *Nat. Nanotechnol.* **2014,** *9,* 111–115.
3. Zhou, H.; Wang, C.; Shaw, J. C.; Cheng, R.; Chen, Y.; Huang, X.; Liu, Y.; Weiss, N. O.; Lin, Z.; Huang, Y.; et al. Large Area Growth and Electrical Properties of P-Type WSe2 Atomic Layers. *Nano Lett.* **2015,** *15,* 709–713.
4. Chen, H.; Li, Y.; Liu, W.; Xu, H.; Yang, G.; Shi, J.; Feng, Q.; Yu, T.; Liu, X.; Liu, Y. High-Temperature Driven Inter-Valley Carrier Transfer and Significant Fluorescence Enhancement in Multilayer WS_2. *Nanoscale Horizons* **2018**, *3*, 598–605.

5. Ross, J. S.; Klement, P.; Jones, A. M.; Ghimire, N. J.; Yan, J.; Mandrus, D. G.; Taniguchi, T.; Watanabe, K.; Kitamura, K.; Yao, W.; et al. Electrically Tunable Excitonic Light-Emitting Diodes Based on Monolayer WSe_2 p-n Junctions. *Nat. Nanotechnol.* **2014,** *9,* 268–272.
6. Gu, J.; Chakraborty, B.; Khatoniar, M.; Menon, V. M. A Room-Temperature Polariton Light-Emitting Diode Based on Monolayer WS_2. *Nat. Nanotechnol.* **2019,** *14,* 1024–1028.
7. Wu, G.; Wang, X.; Chen, Y.; Wang, Z.; Shen, H.; Lin, T.; Hu, W.; Wang, J.; Zhang, S.; Meng, X.; et al. Ultrahigh Photoresponsivity MoS_2 Photodetector with Tunable Photocurrent Generation Mechanism. *Nanotechnology* **2018,** *29,* 485204.
8. Tsai, M.; Su, S.; Chang, J.; Tsai, D.; Chen, C.; Wu, C.; Li, L.; Chen, L.; He, J.; Science, M.; et al. Monolayer MoS_2 Heterojunction Solar Cells. *ACS Nano* **2014,** *8,* 8317–8322.
9. Ugeda, M. M.; Bradley, A. J.; Shi, S. F.; Da Jornada, F. H.; Zhang, Y.; Qiu, D. Y.; Ruan, W.; Mo, S. K.; Hussain, Z.; Shen, Z. X.; et al. Giant Bandgap Renormalization and Excitonic Effects in a Monolayer Transition Metal Dichalcogenide Semiconductor. *Nat. Mater.* **2014,** *13,* 1091–1095.
10. Zhu, B.; Chen, X.; Cui, X. Exciton Binding Energy of Monolayer WS_2. *Scientific reports* **2015,** *5,* 1-5.
11. Chernikov, A.; Berkelbach, T. C.; Hill, H. M.; Rigosi, A.; Li, Y.; Aslan, O. B.; Reichman, D. R.; Hybertsen, M. S.; Heinz, T. F. Exciton Binding Energy and Nonhydrogenic Rydberg Series in Monolayer WS_2. *Phys. Rev. Lett.* **2014,** *113,* 1–5.
12. Park, S.; Mutz, N.; Schultz, T.; Blumstengel, S.; Han, A.; Aljarb, A.; Li, L. J.; List-Kratochvil, E. J. W.; Amsalem, P.; Koch, N. Direct Determination of Monolayer MoS_2 and WSe_2 Exciton Binding Energies on Insulating and Metallic Substrates. *2D Mater.* **2018,** *5,* 025003.

13. Plechinger, G.; Nagler, P.; Kraus, J.; Paradiso, N.; Strunk, C.; Schüller, C.; Korn, T. Identification of Excitons, Trions and Biexcitons in Single-Layer WS_2. *Phys. Status Solidi - Rapid Res. Lett.* **2015,** *9,* 457–461.
14. Singh, A.; Moody, G.; Tran, K.; Scott, M. E.; Overbeck, V.; Berghäuser, G.; Schaibley, J.; Seifert, E. J.; Pleskot, D.; Gabor, N. M.; et al. Trion Formation Dynamics in Monolayer Transition Metal Dichalcogenides. *Phys. Rev. B* **2016,** *93,* 1–5.
15. Mak, K. F.; He, K.; Lee, C.; Lee, G. H.; Hone, J.; Heinz, T. F.; Shan, J. Tightly Bound Trions in Monolayer MoS_2. *Nat. Mater.* **2013,** *12,* 207–211.
16. Steinhoff, A.; Florian, M.; Singh, A.; Tran, K.; Kolarczik, M.; Helmrich, S.; Achtstein, A. W.; Woggon, U.; Owschimikow, N.; Jahnke, F.; et al. Biexciton Fine Structure in Monolayer Transition Metal Dichalcogenides. *Nat. Phys.* **2018,** *14,* 1199–1204.
17. Wood, R. E.; Lloyd, L. T.; Mujid, F.; Wang, L.; Allodi, M. A.; Gao, H.; Mazuski, R.; Ting, P. C.; Xie, S.; Park, J.; et al. Evidence for the Dominance of Carrier-Induced Band Gap Renormalization over Biexciton Formation in Cryogenic Ultrafast Experiments on MoS_2 Monolayers. *J. Phys. Chem. Lett.* **2020,** *11,* 2658–2666.
18. Lee, H. S.; Kim, M. S.; Kim, H.; Lee, Y. H. Identifying Multiexcitons in MoS_2 Monolayers at Room Temperature. *Phys. Rev. B* **2016,** *93,* 140409.
19. Castellanos-Gomez, A.; Quereda, J.; Van Der Meulen, H. P.; Agraït, N.; Rubio-Bollinger, G. Spatially Resolved Optical Absorption Spectroscopy of Single- and Few-Layer MoS_2 by Hyperspectral Imaging. *Nanotechnology* **2016,** *27,* 115705.
20. Kufer, D.; Nikitskiy, I.; Lasanta, T.; Navickaite, G.; Koppens, F. H. L.; Konstantatos, G. Hybrid 2D-0D MoS_2-PbS Quantum Dot Photodetectors. *Adv. Mater.* **2015,** *27,* 176–180.

21. Wu, H.; Si, H.; Zhang, Z.; Kang, Z.; Wu, P.; Zhou, L.; Zhang, S.; Zhang, Z.; Liao, Q.; Zhang, Y. All-Inorganic Perovskite Quantum Dot-Monolayer MoS_2 Mixed-Dimensional van Der Waals Heterostructure for Ultrasensitive Photodetector. *Adv. Sci.* **2018,** *5,* 1801219.
22. Shen, T.; Li, F.; Zhang, Z.; Xu, L.; Qi, J. High-Performance Broadband Photodetector Based on Monolayer MoS_2 Hybridized with Environment-Friendly $CuInSe_2$ Quantum Dots. *ACS Appl. Mater. Interfaces* **2020,** *12,* 54927–54935.
23. Zhang, S.; Wang, X.; Chen, Y.; Wu, G.; Tang, Y.; Zhu, L.; Wang, H.; Jiang, W.; Sun, L.; Lin, T.; et al. Ultrasensitive Hybrid MoS_2-ZnCdSe Quantum Dot Photodetectors with High Gain. *ACS Appl. Mater. Interfaces* **2019,** *11,* 23667–23672.
24. Xu, Z.; Lin, S.; Li, X.; Zhang, S.; Wu, Z.; Xu, W.; Lu, Y.; Xu, S. Monolayer MoS_2/GaAs Heterostructure Self-Driven Photodetector with Extremely High Detectivity. *Nano Energy* **2016,** *23,* 89–96.
25. Shin, D. H.; Jung, D. H.; Kim, Y.; Lee, C.; Wang, X. L.; Choi, S. H. High-Speed Heterojunction Photodiodes Made of Single- or Multiple-Layer MoS_2 Directly-Grown on Si Quantum Dots. *J. Alloys Compd.* **2020,** *820,* 153074.
26. Fujii, M.; Sugimoto, H.; Kano, S. Silicon Quantum Dots with Heavily Boron and Phosphorus Codoped Shell. *Chem. Commun.* **2018,** *54,* 4375–4389.
27. Sugimoto, H.; Fujii, M. Colloidal Mie resonant silicon nanoparticles. *Nanotechnology* **2021,** *32,* 452001.
28. Higashikawa, Y.; Azuma, Y.; Majima, Y.; Kano, S.; Fujii, M. Integration of Colloidal Silicon Nanocrystals on Metal Electrodes in Single-Electron Transistor. *Appl. Phys. Lett.* **2016,** *109,* 213104.

29. Takada, M.; Inoue, K.; Sugimoto, H.; Fujii, M. Solution-Processed Silicon Quantum Dot Photocathode for Hydrogen Evolution. *Nanotechnology* **2021,** *32,* 485709.
30. Sugimoto, H.; Yamamura, M.; Sakiyama, M.; Fujii, M. Visualizing a Core-Shell Structure of Heavily Doped Silicon Quantum Dots by Electron Microscopy Using an Atomically Thin Support Film. *Nanoscale* **2018,** *10,* 7357–7362.
31. Desai, S. B.; Madhvapathy, S. R.; Amani, M.; Kiriya, D.; Hettick, M.; Tosun, M.; Zhou, Y.; Dubey, M.; Ager, J. W.; Chrzan, D.; et al. Gold-Mediated Exfoliation of Ultralarge Optoelectronically-Perfect Monolayers. *Adv. Mater.* **2016,** *28,* 4053–4058.
32. Adhikari, S.; Kim, J. H.; Song, B.; Doan, M. H.; Tran, M. D.; Gomez, L.; Kim, H.; Gul, H. Z.; Ghimire, G.; Yun, S. J.; et al. Bandgap Renormalization in Monolayer MoS_2 on $CsPbBr_3$ Quantum Dots via Charge Transfer at Room Temperature. *Adv. Mater. Interfaces* **2020,** *7,* 2000835.
33. Pandey, J.; Soni, A. Unraveling Biexciton and Excitonic Excited States from Defect Bound States in Monolayer MoS_2. *Appl. Surf. Sci.* **2019,** *463,* 52–57.
34. You, Y.; Zhang, X. X.; Berkelbach, T. C.; Hybertsen, M. S.; Reichman, D. R.; Heinz, T. F. Observation of Biexcitons in Monolayer WSe_2. *Nat. Phys.* **2015,** *11,* 477–481.
35. Shang, J.; Shen, X.; Cong, C.; Peimyoo, N.; Cao, B.; Eginligil, M.; Yu, T. Observation of Excitonic Fine Structure in a 2D Transition-Metal Dichalcogenide Semiconductor. *ACS Nano* **2015,** *9*, 647–655.
36. Barbone, M.; Montblanch, A. R. P.; Kara, D. M.; Palacios-Berraquero, C.; Cadore, A. R.; De Fazio, D.; Pingault, B.; Mostaani, E.; Li, H.; Chen, B.; et al. Charge-Tuneable Biexciton Complexes in Monolayer WSe_2. *Nat. Commun.* **2018,** *9,* 1-6.

37. Mai, C.; Barrette, A.; Yu, Y.; Semenov, Y. G.; Kim, K. W.; Cao, L.; Gundogdu, K. Many-Body Effects in Valleytronics: Direct Measurement of Valley Lifetimes in Single-Layer MoS_2. *Nano Lett.* **2014,** *14,* 202–206.
38. Kim, M. S.; Yun, S. J.; Lee, Y.; Seo, C.; Han, G. H.; Kim, K. K.; Lee, Y. H.; Kim, J. Biexciton Emission from Edges and Grain Boundaries of Triangular WS_2 Monolayers. *ACS Nano* **2016,** *10,* 2399–2405.
39. Zhang, D. K.; Kidd, D. W.; Varga, K. Excited Biexcitons in Transition Metal Dichalcogenides. *Nano Lett.* **2015,** *15,* 7002–7005.
40. Thilagam, A. Exciton Complexes in Low Dimensional Transition Metal Dichalcogenides. *J. Appl. Phys.* **2014,** *116,* 053523.
41. Mayers, M. Z.; Berkelbach, T. C.; Hybertsen, M. S.; Reichman, D. R. Binding Energies and Spatial Structures of Small Carrier Complexes in Monolayer Transition-Metal Dichalcogenides via Diffusion Monte Carlo. *Phys. Rev. B - Condens. Matter Mater. Phys.* **2015,** *92,* 1–5.
42. Pei, J.; Yang, J.; Wang, X.; Wang, F.; Mokkapati, S.; Lü, T.; Zheng, J. C.; Qin, Q.; Neshev, D.; Tan, H. H.; et al. Excited State Biexcitons in Atomically Thin $MoSe_2$. *ACS Nano* **2017,** *11,* 7468–7475.
43. Chellappan, V.; Pang, A. L. C.; Sarkar, S.; Ooi, Z. E.; Goh, K. E. J. Effect of Phonons on Valley Depolarization in Monolayer WSe_2. *Electron. Mater. Lett.* **2018,** *14,* 766–773.
44. Phillips, R. T.; Lovering, D. J.; Denton, G. J.; Smith, G. W. Biexciton Creation and Recombination in a GaAs Quantum Well. *Phys. Rev. B* **1992,** *45,* 4308–4311.
45. Birkedal, D.; Singh, J.; Lyssenko, V. G.; Erland, J.; Hvam, J. M. Binding of Quasi-Two-Dimensional Biexcitons. *Phys. Rev. Lett.* **1996,** *76,* 672–675.

46. Shahmohammadi, M.; Jacopin, G.; Rossbach, G.; Levrat, J.; Feltin, E.; Carlin, J. F.; Ganière, J. D.; Butté, R.; Grandjean, N.; Deveaud, B. Biexcitonic Molecules Survive Excitons at the Mott Transition. *Nat. Commun.* **2014,** *5,* 1-6.
47. Rossbach, G.; Levrat, J.; Jacopin, G.; Shahmohammadi, M.; Carlin, J. F.; Ganière, J. D.; Butté, R.; Deveaud, B.; Grandjean, N. High-Temperature Mott Transition in Wide-Band-Gap Semiconductor Quantum Wells. *Phys. Rev. B - Condens. Matter Mater. Phys.* **2014,** *90,* 1–5.
48. Berg, M.; Keyshar, K.; Bilgin, I.; Liu, F.; Yamaguchi, H.; Vajtai, R.; Chan, C.; Gupta, G.; Kar, S.; Ajayan, P.; et al. Layer Dependence of the Electronic Band Alignment of Few-Layer MoS_2 on Si O2 Measured Using Photoemission Electron Microscopy. *Phys. Rev. B* **2017,** *95,* 235406.
49. Hori, Y.; Kano, S.; Sugimoto, H.; Imakita, K.; Fujii, M. Size-Dependence of Acceptor and Donor Levels of Boron and Phosphorus Codoped Colloidal Silicon Nanocrystals. *Nano Lett.* **2016,** *16,* 2615–2620.
50. Keyshar, K.; Berg, M.; Zhang, X.; Vajtai, R.; Gupta, G.; Chan, C. K.; Beechem, T. E.; Ajayan, P. M.; Mohite, A. D.; Ohta, T. Experimental Determination of the Ionization Energies of $MoSe_2$, WS_2, and MoS_2 on SiO_2 Using Photoemission Electron Microscopy. *ACS Nano* **2017,** *11,* 8223–8230.
51. Hao, L.; Liu, Y.; Gao, W.; Han, Z.; Xue, Q.; Zeng, H.; Wu, Z.; Zhu, J.; Zhang, W. Electrical and Photovoltaic Characteristics of MoS_2/Si p-n Junctions. *J. Appl. Phys.* **2015,** *117,* 114502.
52. Feng, Q.; Shi, J.; Yang, W.; Zhong, W.; Li, Y.; Chen, H.; Liu, W.; Xu, H.; Liu, X.; Liu, Y. Engineering Fluorescence Intensity and Electron Concentration of Monolayer MoS_2 by Forming Heterostructures with Semiconductor Dots. *Nanoscale* **2019,** *11,* 6544–6551.

53. Feng, Q.; Li, Y.; Gao, F.; Sun, Y.; Yan, J.; Liu, W.; Xu, H.; Liu, Y. Manipulating Transfer and Separation of Photocarriers in Monolayer WS_2 via CdSe Quantum Dot Doping. *ACS Photonics* **2020,** *7,* 1857–1865.

54. Cunningham, P. D.; Hanbicki, A. T.; McCreary, K. M.; Jonker, B. T. Photoinduced Bandgap Renormalization and Exciton Binding Energy Reduction in WS_2. *ACS Nano* **2017,** *11,* 12601–12608.

55. Bhanu, U.; Islam, M. R.; Tetard, L.; Khondaker, S. I. Photoluminescence Quenching in Gold-MoS_2 Hybrid Nanoflakes. *Sci. Rep.* **2014,** *4,* 1-5.

56. Li, M.; Yao, J.; Wu, X.; Zhang, S.; Xing, B.; Niu, X.; Yan, X.; Yu, Y.; Liu, Y.; Wang, Y. P-Type Doping in Large-Area Monolayer MoS_2 by Chemical Vapor Deposition. *ACS Appl. Mater. Interfaces* **2020,** *12,* 6276–6282.

57. Mouri, S.; Miyauchi, Y.; Matsuda, K. Tunable Photoluminescence of Monolayer MoS_2 via Chemical Doping. *Nano Lett.* **2013,** *13,* 5944–5948.

58. Thiessen, A. N.; Ha, M.; Hooper, R. W.; Yu, H.; Oliynyk, A. O.; Veinot, J. G. C.; Michaelis, V. K. Silicon nanoparticles: Are they crystalline from the core to the surface? *Chem. Mater.* **2019,** *31,* 678-688.

59. Nomoto, K.; Sugimoto, H.; Breen, A.; Ceguerra, A. V.; Kanno, T.; Ringer, S. P.; Wurfl, I. P.; Conibeer, G.; Fujii, M. Atom probe tomography analysis of boron and/or phosphorus distribution in doped silicon nanocrystals. *J. Phys. Chem. C* **2016,** *120,* 17845-17852.

60. Sugimoto, H.; Yamamura, M.; Fujii, R.; Fujii, M. Donor–acceptor pair recombination in size-purified silicon quantum dots. *Nano Lett.* **2018,** *18,* 7282-7288.

TOC Graphic